Electronic structures of iron-bearing oxidic minerals at high pressure

J. A. TOSSELL

*Department of Chemistry, University of Maryland,
College Park, Maryland 20742*

Abstract

The SCF-xα Scattered Wave Cluster Molecular Orbital Method is used to calculate the electronic structure of the square planar FeO_4^{6-} oxyanion, in both its quintet high spin and singlet low spin states. The order of the predominantly Fe3d crystal-field-type orbitals is calculated to be $x^2-y^2 > xy > xz,yz > z^2$ (with the ligands lying along the x,y axes), in agreement with experiment. The crystal-field-type orbitals differ substantially in %Fe character as a function of both symmetry and spin type. Calculated optical transition energies for the quintet state at R = 2.003 Å are in fair agreement with one atmosphere experimental data. In the singlet state (R = 2.003 Å) spectral transition energies are reduced while the Mössbauer isomer shift increases. Studies on the quintet state at Fe–O distances of 2.03, 2.003, 1.98, and 1.93 Å show a calculated increase in $d_{x^2-y^2} - d_{z^2}$ separation in close agreement with the crystal field R^{-5} distance-dependence law, even though the orbitals involved are only about half metal in character. However, the separation of the spin-up and spin-down xz,yz crystal-field-type orbitals also increases as the Fe–O distance is decreased. The calculations clearly indicate that a quintet → singlet transition will *not* occur at Fe–O distances as small as 1.93 Å. This is apparently consistent with high pressure X-ray studies showing distortion of the Fe site, although a parameterized crystal field calculation based on the high-pressure crystal-structure data does not give good agreement with the experimental optical spectra. MO results are also presented for the FeO_6^{9-} and FeO_6^{10-} clusters at Fe–O distances of 2.17, 2.06, and 1.95 Å. Calculated trends in crystal field energies are again in agreement with the R^{-5} law while O → Fe metal charge-transfer energies are found to initially increase as Fe–O distance is reduced, but to decrease at smaller distances for FeO_6^{10-}. The covalency and width of the valence region also increase strikingly. Analysis of orbital energy trends shows that the energies of a number of different orbital sets must be considered in estimating equilibrium Fe–O distances in the Fe oxides. Differences in the energies of the various orbital sets are discussed for square planar, tetrahedral, and octahedral Fe^{2+} at normal internuclear distances to illustrate this point. Based upon calculated trends in crystal field spectra, spin pairing in octahedral Fe^{2+} compounds is again predicted to occur at mantle pressures. Uncertainties in the molar volumes of high and low spin Fe^{2+}, however, make prediction of the transition pressure very difficult. Finally, the large calculated changes in bond character for the compressed Fe oxides are contrasted with the very small changes calculated for compressed MgO.

Introduction

The SCF xα Scattered Wave Cluster Molecular Orbital Method (Johnson, 1973) has recently been used to calculate the electronic structures of a number of transition metal oxides at normal internuclear distances (Tossell, Vaughan, and Johnson, 1974; Vaughan, Tossell, and Johnson 1974). Calculated optical and X-ray spectral energies were in reasonable agreement with experiment. The crystal field model has recently been employed to calculate the energies of crystal field transitions in Fe-bearing silicate min-

erals at 1 atm (Wood and Strens, 1972) and at high pressures (Gaffney, 1972). Concurrently a great deal of experimental data has been obtained on the high pressure optical spectra of many Fe-bearing minerals (Balchan and Drickamer, 1959; Mao and Bell, 1972; Abu-Eid, 1974; Shankland, Duba, and Woronow 1974).

Experimental shifts in the energies of spin-allowed crystal field bands are in reasonable agreement with those predicted from crystal field theory (Drickamer and Frank, 1973), but the crystal field model yields no explanation for observed trends in the energy and

intensity of oxygen → metal charge-transfer spectra since it treats only the metal-type orbitals. In order to explain the observed data the SCF xα MO method has been applied to the iron oxyanions FeO_4^{6-} (D_{4h} symmetry) and FeO_6^{10-}, FeO_6^{9-} (O_h symmetry) at both normal and reduced internuclear distances. The FeO_4^{6-} results can be applied specifically to the rare mineral gillespite (Pabst, 1943), whose high pressure spectrum has been thoroughly studied (Abu-Eid, Mao, and Burns, 1973). The octahedral oxyanions are appropriate models for a number of different minerals, such as the pyroxenes and olivines, some of which have been studied at high pressure (Shankland et al, 1974; Balchan and Drickamer, 1959).

Spectra of Fe-bearing minerals at high pressure

Gillespite, $BaFeSi_4O_{10}$, is a rare mineral which contains Fe^{2+} in square planar coordination with oxygen [R(Fe–O) = 1.995 Å] (Hazen and Burnham, 1975). The crystal-field splitting for Fe^{2+} in gillespite (~19,000 cm^{-1} or 19 KK) (Burns, 1970) is larger than that found in any other Fe mineral and is almost as large as the difference in energy of the majority-and minority-spin crystal-field orbitals of Fe^{2+}, which is approximately equal to the energy of the spin-forbidden crystal-field transitions, observed between 20 and 23 KK in Fe minerals (Burns, 1970). As is well known, crystal-field splittings increase as R(Fe–O) decreases, the increase being approximately as predicted by the R^{-5} law of crystal field theory. The spin splitting on the other hand, is usually assumed to decrease as R decreases. Therefore, at some reduced R(Fe–O) the crystal-field splitting should become larger than the pairing energy, which is proportional to the spin splitting. This will cause a change in spin state from the normal quintet state of Fe^{2+} to a singlet state with all electrons paired, *if* the above assumptions are correct and if no prior process intervenes.

Spin pairing in Fe^{2+} minerals at high pressure was first predicted by Fyfe (1960). In 1966 Strens showed that the spectrum of gillespite changed dramatically above 26 kbar applied pressure; he attributed this change to a transformation to the low spin state. Inconsistencies in his experimental data led Abu-Eid et al (1973) to repeat the high pressure optical absorption experiments. For light with the electric vector polarized parallel to the four-fold axis of the FeO₄ group, the color of gillespite was found to change from bright red below 26 kbar to bright blue above. The visible absorption spectrum shows two peaks,

both of which shift gradually to higher energy as pressure is applied and then broaden, intensify, and shift to lower energy above the transition point at 26 kbar. High pressure Mössbauer studies (Tossell and Vaughan, unpublished results) gave a spectrum at high pressure consisting of two doublets, indicative of Fe in two electronic states or coordination sites. The parameters (relative to stainless steel) are an isomer shift of 0.87 mm/sec and quadrupole splitting of 0.64 mm/sec for the inner doublet and an isomer shift of 1.13 mm/sec and a quadrupole splitting of 2.02 mm/sec for the outer doublet. The parameters of the inner doublet are essentially identical to those for gillespite at 1 atm; the higher isomer shift for the outer doublet is indicative of a reduced electron density at the Fe nucleus while the increased quadrupole splitting signifies an increase in the asymmetry of the charge distribution. Both the isomer shift and quadrupole splitting values of the outer doublet are within the range expected for tetrahedral Fe^{2+}, raising the possibility that the 26 kbar optical transition (if associated with the Mössbauer transition) involves a change in iron coordination rather than a change in spin state. X-ray crystallographic studies of single crystals of gillespite above 26 kbar have indeed shown a change in space group. However, the distortion of the Fe site from square planar symmetry is small. We will show later that calculations using a parameterized crystal-field model predict the change in coordination site symmetry to produce a smaller change than observed in optical spectra. Therefore, when the present work was initiated, a change in spin state still seemed to be a possible explanation for the properties of the high pressure phase. If such spin changes were to occur generally in Fe minerals, they would have important effects upon solubility relations in the mantle (Gaffney, 1972). Therefore a determination of the cause of the 26 kbar transition in gillespite is of some geophysical significance.

Several other minerals have also been studied at high pressure. Their optical spectra generally show increased spin-allowed crystal-field energies, relatively constant spin-forbidden crystal-field energies, and either increases or decreases in charge-transfer transition energies, which are often associated with dramatic increases in absorption intensity. Experiment indicates a R^{-5} or $V^{-5/3}$ power law for crystal field splittings to be essentially correct, and small deviations from $V^{-5/3}$ dependence have been attributed to differences between local and bulk compressibility, thus suggesting that such deviations can be used as a measure of compressibility

differences (Abu-Eid, 1974). It is often assumed that the success of the $V^{-5/3}$ law verifies the crystal-field theory assumption of the lack of covalent mixing of $M3d$ and ligand orbitals. This argument is invalid, as will be demonstrated later using the MO calculations.

Spin-forbidden crystal-field bands show no systematic dependence on pressure for oxidic minerals, although for more covalent ligands a general decrease in energy is observed at high pressure. Abu-Eid (1974) has found no change in spin-forbidden bands of Fe^{3+} in andradite at high pressure, while Shankland et al (1974) find only very small increases or decreases in spin-forbidden energy for Fe^{2+} in olivines, pyroxenes, and garnets.

In the high-valence-state oxyanions MnO_4^- and CrO_4^{2-}, Bentley and Drickamer (1961) observed increased energies for charge-transfer absorption at pressures <100 kbar while Abu-Eid (1974) has observed large increases in intensity and shifts of the absorption edge to lower energy at high pressures. Mao and Bell (1974) have observed large increases in $M \rightarrow M$ charge-transfer intensity at high P, along with small decreases in transition energy, and have used this effect to distinguish between crystal-field and charge-transfer absorptions.

Calculation of the electronic structure of square planar FeO_4^{6-}

The SCF Xα MO method has been previously described in this journal (Tossell et al, 1974) and has recently been employed in the study of the square planar complexes, $CuCl_4^{2-}$ (Johnson and Wahlgren, 1972) and $PtCl_4^{2-}$ (Messmer, Interrante, and Johnson, 1974). Statistical exchange parameters (α) and sphere radii are the required input parameters to the SCF xα calculation. The parameter values employed in the calculations reported here are given in the appendix. The result of a SCF Xα MO calculation is a set of one-electron molecular orbitals, which are characterized by their energy and the distribution of their electron density in space. The MO diagram obtained for the quintet spin state of square planar FeO_4^{6-} at $R(Fe-O)$ = 2.003 Å (1 atm Fe–O distance from Wainwright, 1969, now supplanted by Hazen and Burnham, 1975) is shown in Figure 1. Although the energies of all 64 electrons in the system were calculated explicitly, only the valence-region orbitals of $O2p$ and $Fe3d$, $4s$, $4p$ character are shown in the figure, where they are labeled according to the irreducible representations of the D_{4h} point group with the oxygens lying along the x and y axes. The MO diagram for the quintet state is complicated by the splitting of majority spin

(up) and minority spin (down) orbitals, which is several eV in magnitude for the metal-type orbitals.

The ordering of the crystal-field type orbitals in D_{4h} metal complexes has long been a topic of dispute. The order $d_{x^2-y^2}(b_{1g}) > d_{xy}(b_{2g}) > a_{1g}(d_{z^2}) > e_g(d_{xz,y^2})$ is predicted by crystal field theory (Wood and Strens, 1972). However the inclusion of covalency effects generally gives an order $b_{1g}(d_{x^2-y^2}) > b_{2g}(d_{xy}) > e_g(d_{xz,yz}) > a_{1g}(d_{z^2})$ (Basch and Gray, 1967). This order was found by Messmer et al (1974) for $PtCl_4^{2-}$ and the calculated order of crystal-field orbitals for FeO_4^{6-} is the same, namely, $(4)b_{1g} > (2)b_{2g} > (2)b_{2g} > (7)a_{1g}$, where the numbers of the crystal field MO's are also given. Burns, Clark, and Stone (1966), in an analysis of the polarized absorption spectrum of gillespite, demonstrated conclusively that the lowest energy crystal-field orbital was the a_{1g} and concluded that the orbital ordering was almost certainly $b_{1g} > b_{2g} > e_g > a_{1g}$. Therefore the SCF X$\alpha$ calculation is in agreement with experiment. In the ground state of D_{4h} FeO_4^{6-}, the spin-up $7a_{1g}, 2e_g, 2b_{2g}$, and $4b_{1g}$ orbitals are completely filled by five (spin-up) electrons, while the sixth d electron (spin-down) occupies the $7a_{1g}\downarrow$ orbital, the highest energy occupied orbital of the system. We abbreviate this configuration as $(a_{1g})^2(e_g)^2(b_{2g})^1(b_{1g})^1$. All the orbitals below the crystal-field set are completely occupied. The lowest energy orbitals shown on the diagram are the M–O bonding orbitals ($1b_{2g}\uparrow - 3b_{1g}\downarrow$) and above these are the $O2p$ nonbonding orbitals ($1b_{2u} - 6e_u$). The crystal-field-type $M3d-O2p$ antibonding orbitals generally are highest in energy although the $7a_{1g}\uparrow$ lies below the $O2p$ nonbonding set. A striking feature of the MO diagram is the very small splitting (1.55 eV) of the $5e_u$ and $6e_u$ orbitals, corresponding to the $Fe4p, O2p$ bonding orbital and an $O2p$ nonbonding orbital respectively. In FeO_6^{10-}, at a Fe–O distance of 2.17 Å, the separation of the analogous $5t_{1u}$ and $6t_{1u}$ orbitals is 4.75 eV. Similarly, the MO charge distributions show almost no Fe character in the $5e_u$ orbital. Therefore Fe4p covalency is much smaller in the square planar than in the octahedral case. The same result apparently holds for the Fe4s covalency, since the $6a_{1g}$ orbital, with possible Fe3d and $4s$ character, is higher in energy relative to the $O2p$ nonbonding set than is the a_{1g} in octahedral FeO_6^{10-}, for which a_{1g} symmetry orbitals possess only s character on Fe. On the other hand, Table 1 also shows that the mixing of $M3d$ and $O2p$ orbitals in the crystal-field orbital set is extremely large for FeO_4^{6-} (D_{4h}), being somewhat larger than that in FeO_6^{10-} or tetrahedral FeO_4^{6-}. The square planar Fe^{2+} ion therefore shows slightly
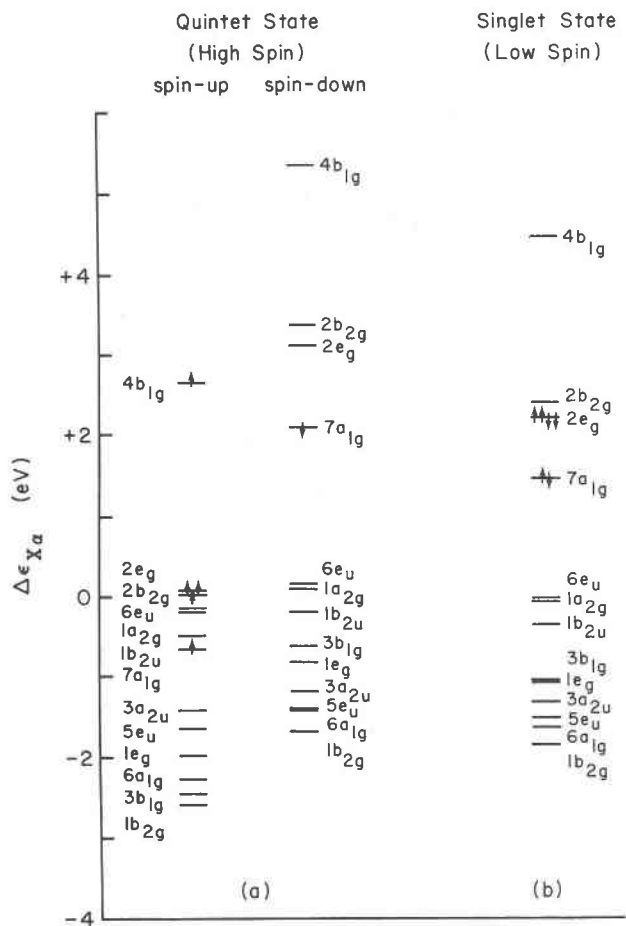
FIG. 1. MO diagrams for (a) quintet and (b) singlet states of square planar FeO_4^{6-}, $R(Fe–O) = 2.003$ Å. (Occupancies of crystal field orbitals are shown by vertical arrows).

greater Fe$3d$ covalency and much smaller Fe$4s,4p$ covalency than do the other coordinations. The influence of atomic properties upon the MO diagram for a square planar cluster may be seen by comparing the MO diagrams of FeO_4^{6-} and $PtCl_4^{2-}$. The calculated MO diagrams are qualitatively similar in that both show very large crystal-field splittings and strong mixing of $M3d$ and ligand orbitals. There are some differences in the order of the highest filled-ligand nonbonding orbitals and in the order of the metal d bonding orbitals. More importantly, the metal derived orbitals in FeO_4^{6-} are consistently about 2–3 eV higher in energy relative to the ligands than in the $PtCl_4^{2-}$ case. Concomitantly, the crystal-field type orbitals contain somewhat more metal character while the metal bonding orbitals have rather little $3d$ character. In $PtCl_4^{2-}$ the percentage of metal $3d$ character in the two sets of orbitals

is similar. These differences are qualitatively understandable if we note that relative to ionization potential, Pt > Fe and O > Cl; hence the Pt-type and Cl-type orbitals in $PtCl_4^{2-}$ will be closer in energy than the Fe- and O-type orbitals in FeO_4^{6-}. The amount of mixing between two atomic orbitals in the formation of a molecular orbital increases as the atomic orbital energies approach each other, as expected.

The accuracy of the calculated orbital energies for the crystal-field-type orbitals can be determined by comparing optical excitation energies calculated using the transition state concept (Slater, 1972) with experimental values. The comparison (Table 2) indicates that the crystal-field splitting is exaggerated by the SCF-Xα calculation to much the same extent as previously found for the octahedral oxides (Tossell *et al* 1974). But note that the estimated crystal field splitting (19 K K) is smaller than the $a_{1g} \rightarrow b_{1g}$ spectral energy since the spectral energy contains the energy contribution of the vibrational transition through which the $g \rightarrow g$ transition is allowed by vibronic coupling.

It is important to note at this point that the SCF-Xα is a one-electron or independent-particle method which gives distinct energies for various electron configurations, such as $(a_{1g}\uparrow)(e_g\uparrow)^2(b_{2g}\uparrow)(b_{1g}\uparrow)(a_{1g}\uparrow)$ in square planar FeO_4^{6-} or $(2t_{2g}\uparrow)^3(3e_g\uparrow)^2(2t_{2g}\uparrow)$ in octahedral FeO_6^{10-}. However, a given configuration generally gives rise to more than one electronic term, unless the symmetry of the point group is low or the total spin of the configuration is large. Term energies could be calculated from the SCF Xα electronic configurations using standard multiplet theory, but such calculations would be difficult and have not yet been implemented. Therefore, at present we cannot usually identify differences of SCF Xα configuration energies with term energy differences observed spectroscopically. Square planar FeO_4^{6-} is a special case, however, in which transitions between the crystal field orbitals correspond uniquely to transitions between electronic states. This result occurs because the direct products of the irreducible representations of the initial state orbital (a_{1g}) and the various final state orbitals correspond to unique irreducible representations; therefore calculated (transition state) orbital-energy differences will correspond directly to observed term differences. For octahedral Fe^{2+} the electron configurations of highest total spin correspond to unique terms, *i.e.* $(2t_{2g}\uparrow)^3(3e_g\uparrow)^2(2t_{2g}\downarrow)$ to $^5T_2$ and $(2t_{2g}\uparrow)^3(3e_g\uparrow)^2(3e_g\downarrow)$ to ^5E, so that the orbital energy difference $2t_{2g}\downarrow - 3e_g\downarrow$ corresponds to the difference of $^5T_2$ and ^5E term energies, $10 Dq$ (or Δ). For

TABLE 1. Electron Density Distribution in FeO_4^{6-} (D_{4h}) in Percent (R(Fe–O) = 2.003 Å)

	High Spin $(a_{1g})^2(e_g)^2 b_{2g} b_{1g}$							Low Spin $(a_{1g})^2(e_g)^4$		
	Fe*	O**	INT***		Fe	O	INT		Fe	O	INT
$4b_{1g}\uparrow$	38	56	5	$4b_{1g}\downarrow$	68	27	4	$4b_{1g}$	63	32	4
$2b_{2g}\uparrow$	55	33	11	$2b_{2g}\downarrow$	82	8	10	$2b_{2g}$	80	11	9
$2e_g\uparrow$	39	49	12	$2e_g\downarrow$	79	10	11	$2e_g$	77	13	10
$7a_{1g}\uparrow$	51	20	29	$7a_{1g}\downarrow$	56	42	0	$7a_{1g}$	65	0	34
$1e_g\uparrow$	52	29	19	$1e_g\downarrow$	7	68	24	$3b_{1g}$	30	61	9
$6a_{1g}\uparrow$	37	47	15	$6a_{1g}\downarrow$	7	67	25	$1e_g$	10	65	23
$3b_{1g}\uparrow$	55	36	8	$3b_{1g}\downarrow$	24	65	9	$6a_{1g}$	9	68	23
$1b_{2g}\uparrow$	38	56	5	$1b_{2g}\downarrow$	6	64	28	$1b_{2g}$	9	63	27

* *percent electron density inside the Fe sphere.*
** *percent electron density inside the O sphere.*
*** *percent electron density in the interatomic region.*

the octahedral compounds spin-flip transitions such as $2t_{2g}\uparrow$–$2t_{2g}\downarrow$ do not, however, produce unique terms. For example, in Fe^{3+} the configuration $(2t_{2g}\uparrow)^2(3e_g\uparrow)^2(2t_{2g}\downarrow)$ spans the terms $^4A_1, {}^4A_2, {}^4T_1, {}^4T_2$, and ^4E. Conversely the above terms correspond to linear combinations of more than one electron configuration. Therefore the spin-flip transitions do not correspond to transitions between discrete electronic states. However, since the energies of the above terms depend primarily upon the Racah parameters B and C, it is evident that an increase in the spin flip energy $2t_{2g}\uparrow$–$2t_{2g}\downarrow$ (or $3e_g\uparrow$–$3e_g\downarrow$) will probably correspond to an increase in B and to an increase in energy of the spin-forbidden peaks (in particular those corresponding to the $^4A, {}^4E$ states of Fe^{3+}).

Differences between high spin and low spin states of square planar FeO_4^{6-}

A SCF $x\alpha$ calculation was also performed on the low-spin singlet state of FeO_4^{6-} with electron configuration $(a_{1g})^2(e_g)^4$ at $R = 2.003$ Å; the MO diagram is shown in Figure 1b. A reasonable initial assumption would be that the orbitals of the singlet state would show properties similar to those of the average of the spin-up and spin-down orbitals of the quintet state. The energies of the orbitals with no metal $3d$ character are closely equal to the average of their spin-up and spin-down energies in the quintet state. However the crystal-field-type orbitals of the singlet are generally about 0.8 eV higher in energy than the average of their quintet values. The percentage of Fe$3d$ character in the crystal field orbitals is

much larger for the singlet than for the average of the spin-up and spin-down orbitals of the quintet. The $7a_{1g}$–$4b_{1g}$ separation in the singlet state is also smaller than either the spin-up or spin-down separations for the quintet state. Therefore the spin splitting in the quintet state does not merely cause a symmetric splitting of the orbitals energies and compositions about their singlet values. The crystal field orbitals are destabilized, their covalency reduced, and their splitting decreased in the singlet state.

Inspection of the percentage compositions of the crystal-field-type orbitals for the two spin states suggests that the number of electrons in the Fe$3d$ orbital is also larger in the singlet state. The SCF $x\alpha$ results show an increase in the number of electrons within the Fe sphere from 23.615 in the quintet state to 23.735 in the singlet. Most of this increase is a result of increased Fe$3d$ electron density. According to the qualitative theory of the Mössbauer isomer shift, such an increase in Fe$3d$ character should produce a decrease in s electron density at the nucleus and consequently a higher isomer shift. Extrapolating from SCF $x\alpha$ electron densities calculated near the nucleus, according to the method of Ellis and Averill (1974), we indeed find a smaller density at the nucleus, $\rho_s(0)$, in the singlet state (11874.70 electrons/au^3 vs 11874.86 in the quintet state). However, as stated by Ellis, the changes in $\rho_s(0)$ calculated using this extrapolation procedure are much smaller than the experimental, given accepted values for the percentage change in the Fe nuclear radius between ground and excited states. Our analysis must thus remain qual-

itative until improved schemes are developed for calculating the electron density at the nucleus from the SCF-Xα orbitals. However, the singlet state does qualitatively show a smaller $\rho_s(O)$ and a larger isomer shift.

As noted, the separation of the crystal field a_{1g} and b_{1g} orbitals is reduced in the singlet state. The qualitative explanation for this effect lies partly in the lowering of the relative energy of the b_{1g} orbital, resultant upon moving an electron from it to the e_g, and partly in the reduction in covalency of the crystal field type orbitals. Therefore the calculations indicate that a transition to the singlet state would lead to a somewhat higher Mössbauer isomer shift and a reduced energy for the $a_{1g} \rightarrow b_{1g}$ (and b_{2g}) transitions, as is shown in Table 2.

A quintet-singlet spin change therefore generates changes in the optical and Mössbauer spectra which show the right experimental trend but are in poor quantitative agreement with the gillespite high pressure data. Additionally, the failure to observe additional spectral peaks in the 26 kbar spectrum argues strongly against a spin transition. The low-spin configuration should show $e_g \rightarrow b_{1g}$ transitions in both polarized spectra (Burns *et al*, 1966), at energies about 3 KK (or more) less than that for the $a_{1g} \rightarrow b_{1g}$ transition. No such feature is seen in the high pressure spectrum.

Calculated electronic structure of square planar FeO$_4^{6-}$ at high pressure

In order to directly model the effects of pressure on perfect square planar FeO$_4^{6-}$, SCF Xα calculations were performed at $R = 2.03$, 2.003, 1.98, and 1.93 Å. Such calculations provide a basis for predicting the electronic state of square planar Fe^{2+} at high pressure. No qualitative changes occurred in the MO diagram, but sizable quantitative shifts were observed; trends are illustrated in Table 3 and Figure 2. The $7a_{1g} \downarrow \rightarrow 4b_{1g} \downarrow$ transition, which yields the high energy crystal field peak, steadily increases in energy at a rate in good agreement with the R^{-5} law as shown in Table 3. The energies given are ground state eigenvalue differences, but these differ only slightly from the transition state eigenvalue differences and the trends are not affected. It is initially surprising to observe that the R^{-5} law holds so well for a transition from an orbital of about 60 percent Fe character to one with 40 percent Fe character. Clearly, agreement with the R^{-5} law does not establish the validity of the ionic model. Molecular orbital calculations showing substantial covalency can and do give essentially the R^{-5} result. The $2e_g$ spin splitting also increases at smaller R. This violates the rule of thumb that the Racah parameters of transition metal cations generally decrease at high pressure. However, as suggested earlier, this rule is appropriate only for polarizable ligands and does not necessarily apply to Fe oxides. The $7a_{1g} \uparrow - 4b_{1g} \uparrow$ splitting also increases with smaller R, but in a less regular way. Therefore the R^{-5} law seems to apply most accurately to the spin-down crystal-field orbitals which are energetically well separated from the ligand orbitals (and which, for Fe^{2+}, alone determine the optical spectral energies). The width of the valence region is also slightly greater for the $R = 1.93$ Å case; the $5e_u$–$6e_u$ separation increases from 1.56 to 1.76 eV. The energy for the charge transfer transition $6e_u \downarrow \rightarrow 2e_g \downarrow$ also increases at small Fe–O distances; in fact the entire manifold of crystal field orbitals is raised, with the average energy, or baricenter, of the spin-down crystal-field orbitals being raised by 0.6 eV. Although this destabilization of the spin-down crystal field is substantial, it is only about 20 percent of that predicted from the ionic model assuming full formal charges of 2− on the oxygens. On the other hand, the crystal field orbitals certainly do not show lowered energies and greatly increased delocalization at the smaller distances. The ionic model prediction of raised crystal-field-orbital baricenters is at least qualitatively correct.

In determining whether a change in spin state will occur in FeO$_4^{6-}$ at reduced R, one should focus upon the relative energies of the $2b_{2g} \uparrow$ and $2e_g \downarrow$ orbitals. Only if that of $2e_g \downarrow$ falls below $2b_{2g} \uparrow$ will the singlet state become stable. This clearly has not happened even at $R = 1.93$ Å. The $7a_{1g} \uparrow - 2b_{2g} \uparrow$ energy difference has increased by only 0.5 eV (10%) from its 2.003 Å value while the $7a_{1g} \uparrow - 7a_{1g} \downarrow$ separation has

TABLE 2. Calculated and Experimental Spectral Energies in Square Planar FeO$_4^{6-}$ (in KiloKaysers)

Calculated Energies ($R = 2.003$ Å)		
	High Spin (Quintet)	Low Spin (Singlet)
Transition		
$7a_{1g} \downarrow \rightarrow 2b_{2g} \downarrow$	11.4	7.7
$7a_{1g} \downarrow \rightarrow 4b_{1g} \downarrow$	27.0	24.2
Experimental Energies		
	1 atm	26 kbar
Transition		
$7a_{1g} \downarrow \rightarrow 2b_{2g} \downarrow$	8.3	7.1
$7a_{1g} \downarrow \rightarrow 4b_{1g} \downarrow$	20.6	18.3

TABLE 3. Effect of Fe–O Distance on Ground State Eigenvalue Differences in Square Planar FeO_4^{6-} (Energies in KiloKaysers)

R(Fe–O) (Å)	2.030	2.003	1.980	1.930
$\Delta\epsilon_{X\alpha}^{R}(7a_{1g}\downarrow - 4b_{1g}\downarrow)$	24.6	26.1	27.8	30.9
$\dfrac{\Delta\epsilon_{X\alpha}^{R}(7a_{1g}\downarrow - 4b_{1g}\downarrow)}{\Delta\epsilon_{X\alpha}^{R}\ =\ 2.030\ (7a_{1g}\downarrow - 4b_{1g}\downarrow)}$	1.00	1.06	1.13	1.26
$\left(\dfrac{R}{2.030}\right)^{-5}.$	1.00	1.07	1.13	1.29
$\Delta\epsilon_{X\alpha}^{R}(2e_g\uparrow - 2e_g\downarrow)$	21.9	24.5	25.8	26.8
$\Delta\epsilon_{X\alpha}^{R}(6e_u\downarrow - 2e_g\downarrow)$	22.7	24.0	25.0	26.8
$\Delta\epsilon_{X\alpha}^{R}(7a_{1g}\uparrow - 4b_{1g}\uparrow)$	23.4	26.9	28.2	30.4

increased by 0.8 eV (4%) and the $7a_{1g}\downarrow - 2e_g\downarrow$ separation by 1.8 eV (22%). Therefore a transition to the singlet state seems impossible, no matter how high the pressure. For transition to the $(a_{1g})^2(e_g)^3(b_{2g})$ triplet state, the requirement is that the $2e_g\downarrow$ fall below the $4b_{1g}\uparrow$. The $7a_{1g}\uparrow - 4b_{1g}\uparrow$ separation increases with smaller R somewhat faster than R^{-5} while the $2e_g\uparrow - 2e_g\downarrow$ increases at about the R^{-5} rate, although in each case the trend is somewhat irregular. The $4b_{1g}\uparrow - 2e_g\downarrow$ separation therefore decreases from 3.7 KK at $R = 2.003$ to 2.7 KK at $R = 1.93$ and a transition to the triplet state at higher pressure is therefore a possibility. The energy of such a transition in the SCF-$x\alpha$ theory is more properly expressed as a difference of one-electron orbital eigenvalues for the transition state of the process, although ground state and transition state eigenvalue differences are usually quite similar. Direct calculation of the $4b_{1g}\uparrow - 2e_g\downarrow$ eigenvalue difference in the transition state gives 2.0 KK, slightly smaller but still clearly positive, indicating that the quintet state remains the more stable. An SCF-$x\alpha$ calculation has been performed for the triplet state to determine the change in optical and Mössbauer parameters to be expected in a quintet → triplet spin change. The $7a_{1g}\downarrow - 4b_{1g}\downarrow$ transition energy decreases by about 0.4 KK from its quintet state value while the number of electrons within the Fe sphere increases by about 80 percent of the quintet to singlet difference. The predicted changes in optical spectral energy for the quintet to triplet transition is therefore considerably smaller than the experimental change

observed at 26 kbar. In addition, in the triplet state transitions of the type $e_g \rightarrow b_{1g}$ would give additional peaks in the spectrum; as previously noted no such features are observed.
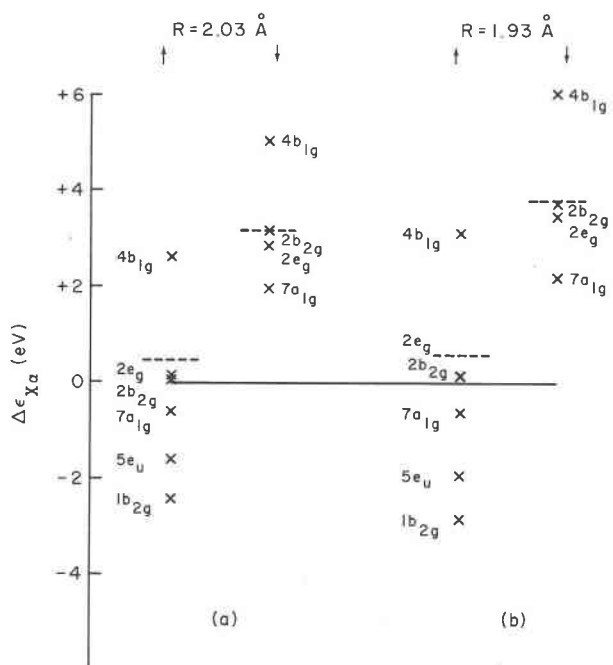

FIG. 2. MO diagrams for quintet state of square planar FeO_4^{6-} at (a) $R(Fe–O) = 2.03$ Å and (b) $R(Fe–O) = 1.93$ Å. (With horizontal line corresponding to constant $6e_u$ energy and broken lines signifying crystal field spin up and crystal field spin down orbital baricenters).

Since a change of spin state is not consistent with either the SCF $X\alpha$ calculations or experimental data, the alternative explanation of a change in site symmetry as the cause of the changes in optical and Mössbauer spectra must be favored. A change in site symmetry has been observed experimentally. Above the 26 kbar transition point, Fe in gillespite lies in a distorted square planar site with twofold symmetry (R.M. Hazen and C. W. Burnham, personal communication, 1975). There are two unique pairs of oxygens whose internuclear vectors are at right angles. The Fe–O distance for the two unique oxygens are indistinguishable within the accuracy of the data, each being 1.965 ± 0.02 Å. The two unique O–Fe–O angles are 158° and 175° and have opposite senses, such that the four oxygens are distorted toward tetrahedral symmetry.

An SCF $X\alpha$ calculation on such a low symmetry cluster would be very expensive, so that molecular quantum mechanical calculations on this system are not presently feasible. Therefore more approximate methods must be used. Recently, methods have been developed for calculating crystal field spectra from the assumed R^{-5} distance dependence of the

TABLE 4

The expressions for d-orbital energies given by Wood and Strens (1972) are

$$E_{z^2} = -0.214\Delta_x - 0.214\Delta_y + 1.028\Delta_z$$
$$E_{x^2-y^2} = +0.614\Delta_x + 0.614\Delta_y - 0.628\Delta_z$$

where $\Delta_x = \sum_i \Delta_o (R_o/R_i)^5 \cos^2 \Theta_i$

is summed over ligands and Θ is angle between M–O and x axis

At 1 atm R(Fe–O) = 1.995 ± 0.003 Å
$\langle$O–Fe–O$\rangle$ = 178°, $\Delta = \Delta_o$
$\Delta_x = \Delta_y = [\cos(1°)]^2 \Delta_o = 0.9997$
$\Delta_z = \cos(89°)^2 \Delta_o = 0.0003$ Å
$E_{x^2-y^2} - E_{z^2} = 1.656\Delta_o$

At 26 kbar (R(Fe–O) = 1.98 ± 0.02(2), 1.95 ± 0.02(2),
av. 1.965 ± 0.02

$\langle$O–Fe–O$\rangle$ = 158° (2), 175° (2)

$\Delta = \Delta_o \left(\dfrac{1.995}{1.965}\right)^5 = 1.0788\Delta_o$

$\Delta_x = [\cos(11°)]^2 (1.0788\Delta_o) = 1.0395\Delta_o$
$\Delta_y = [\cos(2.5°)]^2 (1.0788\Delta_o) = 1.0767\Delta_o$
$\Delta_z = (\cos(87.5°)^2 + \cos(79°)^2 (1.0788\Delta_o) = 0.0207\Delta_o$
$E_{x-y} - E_{z^2} = 1.718\Delta_o$

Crystal structure data from R. M. Hazen and C. W. Burnham, personal communication, 1975.

crystal field splitting combined with empirical parameterization (Wood and Strens, 1972; Gaffney, 1972). Using the expressions of Wood and Strens for the d orbital energies in a distorted octahedron and their equation for the crystal field splitting components along the coordinate axes, one can calculate the expected change in gillespite crystal field energies resulting from the change in coordination site geometry.

Applying the Wood and Strens parameters (Δ_o = 9.75 KK at R_o = 2.135 Å) to the gillespite structure at 1 atm, we calculate $a_{1g} \rightarrow b_{1g}$ and $a_{1g} \rightarrow b_{2g}$ energy differences of 26.0 and 9.0 KK, in quite good agreement with experiment. Unfortunately, as previously noted, the order of the orbitals in the crystal field calculation is $b_{1g}(d_{x^2-y}) > b_{2g}(d_{xy}) > a_{1g}(d_{z^2}) > e_g(d_{xz,yz})$ in disagreement with the SCF $X\alpha$ results and the polarized absorption spectra of Burns *et al* (1966). Apparently the only orbital energy seriously in error in the crystal field calculation is that for the e_g orbital, which is much too low. It thus seems probable that the parameterized crystal field approach will yield reasonable values for the change in $a_{1g} \rightarrow b_{2g}$ and $a_{1g} \rightarrow b_{1g}$ energies as a function of distortion from D_{4h} symmetry. An application of the Wood and Strens model to the crystal structure data for the deformed gillespite II site (above 26 kbar) is outlined in Table 4. The disconcerting result is that the calculated $a_{1g} \rightarrow b_{1g}$ separation is actually larger for the high pressure phase, since the reduction in R(Fe–O), though small, overwhelms the effect of the distortion toward tetrahedral symmetry. The $a_{1g} \rightarrow b_{1g}$ energy in the crystal field model is approximately proportional to $|\cos(\pi - \langle$O–Fe–O$\rangle)|$, which is a very slowly decreasing function for $\langle$O–Fe–O$\rangle$ near 180°. However, significant reductions of crystal field energies have been observed experimentally for Cu(II) chlorides, accompanying distortion from square planar to (distorted) tetrahedral geometry (Willett *et al*, 1974). From Willet's empirical curve of crystal-field transition energy *vs* $\langle$Cl–Cu–Cl$\rangle$ angle and the percent reduction in crystal field energy in gillespite II, we would predict values of about 155° for both $\langle$O–Fe–O$\rangle$ angles. Clearly the two systems are much different, but the trend is in the right direction and of the proper magnitude. Curiously, the application of high pressure to Cu(II) salts often results in tetrahedral $\rightarrow$ square planar geometry changes (Wang and Drickamer, 1973), the opposite to that observed in gillespite. The above evidence thus generally supports the geometry change interpretation of changes in the optical spectra, but the

analysis does not yet yield a quantitatively correct result.

Comparison of energy levels in square planar, tetrahedral, and octahedral Fe^{2+}

The relative energies of the $Fe3d$ crystal-field-type orbitals in different coordination symmetries are given in Table 5. The baricenter of the crystal-field-orbital manifold is relatively constant between the various coordinations. However the separate spin-up and spin-down orbital baricenters differ substantially. The low baricenter energy for the spin up orbitals in D_{4h} geometry is associated with the large $M3d,O2p$ covalency; conversely for the T_d case the smaller amount of covalency gives a high energy for the spin-up baricenter. Comparison of the $Fe3d$ crystal field baricenters and the crystal field splittings indicates that the Fe^{2+} crystal field orbitals are more stable in D_{4h} than in T_d geometry. A similar result is obtained on the basis of the crystal field splittings alone, even if the baricenters are assumed to be the same. Since Fe^{2+} actually prefers T_d to D_{4h} symmetry, variations in the energy of the crystal field orbitals must be compensated by energy variations within other orbitals of the valence band. As previously noted, the stabilization of the bonding orbitals is much less in D_{4h} than in either T_d or O_h geometry. The small $4s,4p$ covalency in the D_{4h} case, giving a small separation of $O2p$ nonbonding and M,O bonding orbitals, will contribute to the relative instability of the square planar configuration. Additionally, in tetrahedral geometry the O–O distances are maximized and the repulsions between the oxygens are therefore minimized. This interoxygen repulsion would result mainly in a shift of the absolute energies of the $O2p$ nonbonding orbital energies. This effect, though small in magnitude per electron, would affect most if not all of the electrons of the system. This effect is ignored in our analysis by virtue of the assumed constancy in energy of the $6e_u,O2p$ nonbonding orbital.

Calculated electronic structure of octahedral FeO_6^{9-} and FeO_6^{10-} at high pressure

SCF-Xα calculations have previously been presented for Fe^{2+} (FeO_6^{10-}) at RFe–O) = 2.17 Å and for Fe^{3+} (FeO_6^{9-}) at R(Fe–O) = 2.06 Å. In each case the occupied valence region MO's could be divided into (1) an $O2s$ nonbonding set ($5a_{1g},4t_{1u},1eg$), (2) a M–O bonding set ($5t_{1u}$, $6a_{1g},1t_{2g},2e_g$), (3) an $O2p$ nonbonding set ($1t_{2u}$, $6t_{1u}$, $1t_{1g}$), and (4) a crystal field set ($2t_{2g}$, $3e_g$). The crystal field orbitals were at lower

TABLE 5. Energies of Crystal Field Orbitals (Relative to Highest Energy $O2p$ Nonbonding Orbital) in Different Coordination Symmetries

	D_{4h} (R = 1.98)	T_d (R = 1.99)	O_h (R = 2.17)
$CF^a\uparrow$	+.42	+1.11	+.64
$CF\downarrow$	+3.42	+3.32	3.67
CF	1.92	2.21	2.15
$\Delta\epsilon$($\downarrow$baricenter lowest $\downarrow$orbital)	-1.33	-0.14	-0.70

^{a}Weighted energy of crystal field orbitals

relative energy in the FeO_6^{9-} case, showed a larger $t_{2g}-e_g$ splitting, and had a wider valence region. SCF-Xα calculations have since been performed for both FeO_6^{10-} and FeO_6^{9-} clusters at Fe–O distances of 2.17 and 2.06 Å and at the reduced distance of 1.95 Å. Some results of the calculations are shown in Table 6.

To separate the effects of number of $3d$ electrons from differing internuclear distance upon the electronic structure of Fe^{2+} and Fe^{3+} oxidic clusters, we shall first compare the FeO_6^{10-} and FeO_6^{9-} clusters at $R = 2.06$ Å. First, we find that the crystal field splitting is greater in the Fe^{3+} case (2.66 vs 2.48 eV, from ground state energies). This is in agreement with the higher expected Fe charge in FeO_6^{9-}. Second, the spin-forbidden transitions are at lower energy in the Fe^{3+} cluster (3.1 vs 3.3 eV for $2t_{2g}\uparrow - 2t_{2g}\downarrow$, 2.7 vs 3.1 eV for $3e_g\uparrow - 3e_g\downarrow$). This result holds despite the larger total spin in the Fe^{3+} case and is indicative of substantially more $Fe3d$ electron delocalization in Fe^{3+}. For both oxidation states the spin forbidden σ type (e_g) transition lies at lower energy than the π type (t_{2g}) and the percentage of metal character is smaller in the e_g than in the t_{2g} orbitals, consistent with the qualitative picture of the $3e_g$ orbital as strongly σ antibonding and the $2t_{2g}$ as weakly π antibonding.

The calculated increase in the $2t_{2g}\downarrow - 3e_g\downarrow$ crystal field splitting at reduced R for both FeO_6^{9-} and FeO_6^{10-} is in reasonable agreement with the R^{-5} law. The $2t_{2g}\uparrow - 2t_{2g}\downarrow$ spin splitting increases slightly for small reductions of R(Fe–O) from the equilibrium values (2.06 for Fe^{3+}, 2.17 for Fe^{2+}) and then continues to increase slightly for Fe^{3+} but decreases sharply for Fe^{2+}. The lowest energy O $\rightarrow$ M charge-transfer transition ($1t_{1g}\downarrow \rightarrow 2t_{2g}\downarrow$) also initially increases in energy for both Fe^{2+} and Fe^{3+}, but reaches a max-

TABLE 6. Variation in Orbital Energy Differences in FeO_6^{10-} and FeO_6^{9-} as a Function of $R(Fe-O)$ (Energies in eV, 1 eV = 8.067 KK)

	FeO_6^{10-}			FeO_6^{9-}		
R =	2.17	2.06	1.95	2.17	2.06	1.95
$\Delta\varepsilon_{X\alpha}^R (3e_g\downarrow - 2t_{2g}\downarrow)$	1.73	2.32	3.22	1.76	2.25	2.99
$\Delta\varepsilon_{X\alpha}^R (3e_g\uparrow - 2t_{2g}\uparrow)$	2.01	2.48	3.14	2.21	2.66	3.28
$\dfrac{\Delta\varepsilon_{X\alpha}^R (3e_g\downarrow - 2t_{2g}\downarrow)}{\Delta\varepsilon_{X\alpha}^{R=2.17} (3e_g\downarrow - 2t_{2g}\downarrow)}$	1.00	1.34	1.86	1.00	1.28	1.70
$(R/2.17)^{-5}$	1	1.30	1.71	1	1.30	1.71
$\varepsilon_{2t_{2g}\uparrow} - \varepsilon_{2t_{2g}\downarrow}$	3.21	3.28	2.65	2.91	3.12	3.17
$\varepsilon_{2t_{2g}\downarrow} - \varepsilon_{1t_{1g}\downarrow}$	2.94	3.28	3.24	1.14	1.40	1.54

imum and then decreases for Fe^{2+}. The striking difference in these trends for Fe^{2+} and Fe^{3+} is clearly associated with the larger reduction of $R(Fe-O)$ from its equilibrium value in the FeO_6^{10-} case. Previous theoretical studies have shown similar trends. In particular, both the SCF $X\alpha$ studies of Ellis and Averill on $FeCl_4^-$ and the CNDO studies of Allen, Clack, and Farrimond (1971) on MnF_6^{2-} show continuous destabilization of the crystal field orbitals relative to the ligand nonbonding orbitals as the $M-L$ distance decreases. The present calculations are the first to show a reduction of $O2p$ nonbonding-crystal-field-orbital separation at greatly reduced $R(M-L)$.

The agreement of the calculated $2t_{2g}\uparrow - 3e_g\uparrow$ splittings with the R^{-5} law is in accord with experiment and again shows that complete ionicity is not a necessary condition for the existence of such a distance-dependence. The initial increase in spin-spin splitting is unexpected, but as discussed earlier is consistent with the experimental data. The experimental data on $O \rightarrow M$ charge-transfer transitions is less straightforward in interpretation. As noted previously, the $O \rightarrow M$ charge-transfer peaks for the permanganate ion do shift slightly to higher energy as the pressure is raised (Bentley and Drickamer, 1961). The observed red shift of the absorption edge for the chromate ion (Abu-Eid, 1974) is therefore probably a result of increased charge transfer intensity rather than of reduced energy for the peak maximum. The calculations indicate that pressure-induced thermal $O^{2-} \rightarrow Fe^{3+}$ charge transfer in oxide minerals (or $Fe^{3+} \rightarrow Fe^{2+}$ reduction) either occurs at very small $R(Fe-O)$, or is not really a result of a decreased separation of the ground state and the charge-transfer excited-state energy minima. Changes in the shape of the potential energy curves for ground and excited state may be the dominant factor in determining the energy at which curve crossing occurs. Alternatively, the rate of thermal transition may be controlled by the transmission probability for passage between potential energy curves at the crossing point. The transmission probability increases directly with the optical transition probability (Hush, 1968) which in turn increases sharply at high pressure. Finally, thermal $O^{2-} \rightarrow Fe^{3+}$ charge transfer, as demonstrated by Mössbauer spectroscopy (Drickamer and Frank, 1973) is observed mainly in Fe compounds with polarizable ligands which experimentally show continuous reduction of $O \rightarrow M$ optical charge-transfer peak energies at high pressures. Pure Fe_2O_3 does not show pressure induced reduction of Fe^{3+}. On the other hand pressure-induced reduction of iron has been demonstrated in the minerals magnesioriebeckite (Burns *et al*, 1966) (in which two of the nearest neighbors of Fe are OH) and in an andradite-uvarovite garnet (Huggins, 1974). Clearly, the question of thermal $O^{2-} \rightarrow Fe^{3+}$ reduction requires further study.

Although electron densities at the nucleus calcu-

lated using present methods are not particularly accurate, they do show the correct trends, *i.e.*, the density at the Fe nucleus in FeO_6^{9-} increases as the Fe–O distance is reduced. ($\rho_s(O)$ = 11874.55, 11875.06, and 11875.78 e/(au)^3 for FeO_6^{9-} at R = 2.17, 2.06, 1.95 Å, respectively). At the same time the spin–spin splitting, related to the Racah parameters, also increases. Therefore the decrease in Fe isomer shift at high pressures is not simply related to a delocalization of the Fe3d electron wavefunctions and may arise primarily from s orbital compression.

Energies of orbital sets as a function of distance in octahedral clusters

Total energies as a function of distance, and derived quantities such as equilibrium internuclear distances and stretching force constants, cannot presently be accurately obtained from the SCF-xα calculations for two basic reasons. First, the FeO$_6$ cluster contains six O atoms for each Fe atom rather than the 1:1 ratio of FeO or the 3:2 ratio of Fe$_2$O$_3$; total energies for the cluster therefore exaggerate the contribution of oxygen-type orbitals. Second, the calculated total energy depends strongly upon the attraction between the negative charge on the anion cluster and the positive charge on the Watson sphere, which is, however, a very crude representation of the non-nearest neighbor atoms. In this approximation the total energy will be equal to the sum of the SCF xα statistical total energy of the cluster and the Coulombic attraction between negatively charged cluster and the positive charge on the enclosing Watson sphere. It is not presently clear whether it is more appropriate to use the full 9+ charge on the Watson sphere or the reduced charge (7.75+) required to simulate the Madelung constant (Vaughan *et al*, 1974). In either case the approximate FeO_6^{9-} total energy does have a minimum at R = 2.04 − 2.08 Å, close to the experimental value. If the Watson sphere term is ignored completely, the equilibrium distance increases to about 2.12 Å. However, the variation of total energy with distance is unreasonably steep. Total energies of −3446.6, −3448.7, and −3445.2 Ryd (1 Ryd = 13.6 eV) are obtained for R(Fe–O) = 2.17, 2.06, 1.95 Å, respectively, using a 9+ Watson sphere charge. Therefore, although the potential curve is qualitatively correct, it needs considerable refinement. In particular, more systematic procedures must be developed for choosing sphere radii and evaluating the Watson sphere term.

Nevertheless, the qualitative features which in-

fluence the total energy can be identified. For example, changes in orbital energies generally make the dominant contribution to changes in the total energy of a system. Therefore an examination of changes in orbital energy relative to a fixed reference level should allow us to identify the various energetic effects. In Figure 3 the orbital energies, with respect to the average energy of the O2p nonbonding orbitals $1t_{1g}$, $6t_{1u}$, and $1t_{2u}$, are shown for FeO_6^{9-} and FeO_6^{10-} at different Fe–O distances. Examining the orbital energy trends, we see that the $6a_{1g}$ and $5t_{1u}$ orbitals are stabilized at small R in both the Fe^{2+} and Fe^{3+} clusters and have almost identical energies for the two oxidation states. Likewise the relative energies of the O2p nonbonding orbitals $1t_{1g}$, $6t_{1u}$, and $1t_{2u}$ are dependent only on Fe–O (or O–O) distance and not on the number of electrons in the Fe crystal-field levels. At an Fe–O distance of 2.17 Å the average energies of the $1t_{2g}$ and $2e_g$ orbitals are about 1 eV lower in the FeO_6^{9-} cluster than in FeO_6^{10-}, but at smaller R these orbitals are destabilized in the Fe^{3+} case and slightly stabilized for Fe^{2+}. The major difference between the two clusters occurs in the energies of the crystal-field-type orbitals, $2t_{2g}\uparrow$, $3e_g\uparrow$, and $2t_{2g}\downarrow$. Of course, in FeO_6^{9-} the $2t_{2g}\downarrow$ orbital is empty and therefore makes no contribution to the energy. In FeO_6^{10-} the energy of this orbital increases steadily as R is reduced, but at a relatively slow rate. The slowness of the change in orbital energy results from the competition between the destabilization of the spin-down orbital baricenter and the increasing crystal-field splitting, which stabilizes the t_{2g} orbital. The largest increase in relative energy is observed for the $3e_g\uparrow$ orbital where the effects of baricenter rise and of increased crystal-field splitting are additive. Although the $3e_g\uparrow$ has about 1.3 eV lower relative energies in the Fe^{3+} case, due to the smaller amount of electron repulsion within the 3d shell, the increase in relative energy at small R is the same for Fe^{3+} and Fe^{2+}. The $2t_{2g}\uparrow$ orbital, on the other hand, shows much less destabilization in the Fe^{3+} case.

The dominant effect upon the relative equilibrium internuclear distances in Fe^{2+} and Fe^{3+} oxides is thus clearly the presence of the $2t_{2g}\downarrow$ electron in FeO_6^{10-}, which is destabilized as R is decreased. The $5t_{1u}$, $6a_{1g}$ bonding orbitals and the O2p nonbonding orbitals are unaffected by the number of Fe3d electrons. The $1t_{2g}$, $2e_g$ bonding orbitals and the $2t_{2g}\uparrow$ crystal field orbital do show slightly different trends in the two clusters but the trends tend to compensate each other energetically. For each oxidation state the equilibrium distance is determined by the competition be-
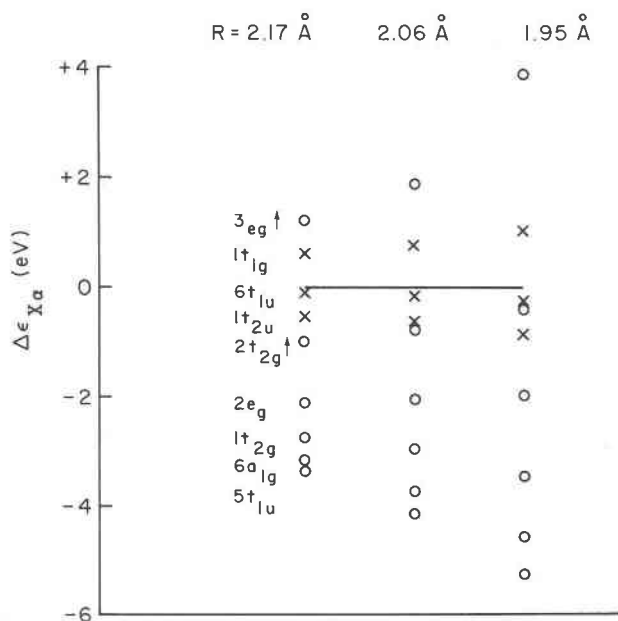
FIG. 3a. Variation of MO energies for FeO_6^{9-} as $R(Fe-\frac{1}{3})$ is decreased from 2.17 to 2.06 to 1.95 Å. (Horizontal line corresponds to constant $1t_{1g}$, $6t_{1u}$, $1t_{2u}$ average energy. Crosses signify $O2p$ nonbonding orbitals; other orbitals are indicated by open circles. Highest occupied orbital is $3e_g\uparrow$ with two electrons).

tween crystal field orbital destabilization and bonding orbital stabilization as R(Fe–O) is decreased.

Determination of the pressure for transition between high and low spin forms of FeO_6^{10-}

To determine the pressure at which high-spin ferrous iron will transform to low-spin ferrous iron in mantle minerals we must evaluate the free energy, G $= E + PV - TS$, for each state of the FeO_6^{10-} system as a function of pressure and temperature. Quantum mechanical calculations and spectral data give information only on the relative internal energies, ΔE, of the various states of the system. To evaluate the free energies we must also consider differences in molar volume, V_m, and molar entropy, S_m, between the two states, as discussed in Ahrens and Syono (1967). The molar volume affects the free energy through the term $P\Delta V_m$, where P is the pressure and ΔV_m the difference in molar volume of the two states. For pure FeO, ΔV_m may be approximated by the product of the 1 atm value of V_m and the percent decrease in $[R(Fe–O)]^3$. For a contraction of the Fe–O distance from 2.17 to 2.01 Å, corresponding to the difference of Fe^{2+} high-spin and low-spin ionic radii give by Shannon and Prewitt (1969), the decrease in the molar volume of FeO would be about 2.6 cm³/mole,

similar to that calculated by Fyfe (1960). However, recent MO calculations on the high-spin and low-spin states of d^6 metal fluorides by Clack and Smith (1974) obtain much smaller differences in high-spin *vs* low-spin equilibrium metal-fluorine distances. For FeF_6^{4-} the calculated difference in equilibrium distance between quintet and singlet state is only 0.03 Å, suggesting a value of about 0.5 cm³/mole for ΔV_m in FeO (if the oxide and fluoride behave similarly). The magnitude of $P\Delta V_m$, expressed in KK, is then approximately: $P\Delta V_m(KK) = 8.3 \times P$ (megabar) $\times \Delta V_m$ (cm³/mole), assuming that ΔV_m is independent of pressure, *i.e.*, that the compressibilities of the two phases are equal.

In the $-T\Delta S_m$ term in the free energy, ΔS has two components. The first is a vibrational component related to the difference in Fe–O vibrational frequency for the high- and low-spin states. No reliable estimate of this term can be given, but it is expected to be small (Strens, 1966). The second component, the difference in electronic entropies, can be estimated simply from the degeneracies of the electronic states (Lewis and Randall, 1961)—$5 \times 3 = 15$ for the $^5T_{2g}$ high-spin state and 1 for the $^1A_{1g}$ low-spin state. The difference in electronic entropy is $\Delta S = R$ ln 15 $\simeq 6.3$ cal/mole°K. At room temperature $-T\Delta S_m$
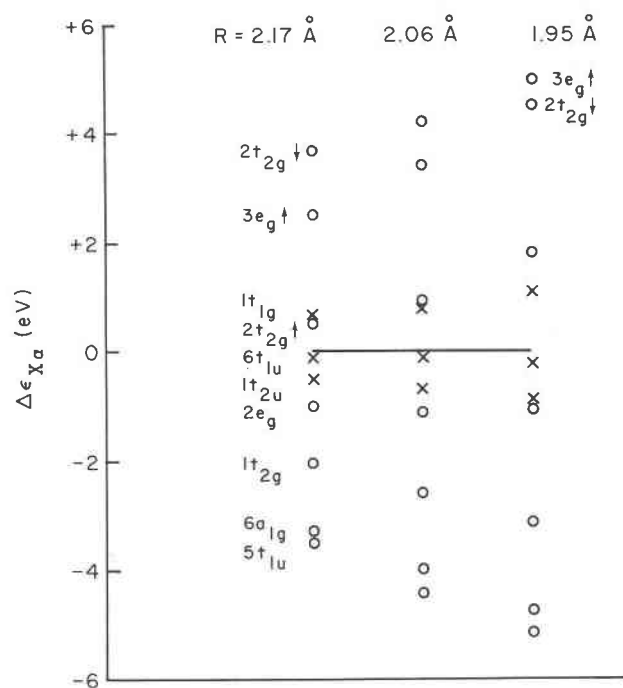

FIG. 3b. Variation of MO energies for FeO_6^{10-} as R(Fe–O) is decreased from 2.17 to 2.06 to 1.95 Å (with symbols as in Figure 3a; highest occupied orbital is $2t_{2g}\downarrow$ with one electron).

TABLE 7. Magnitudes of the Various Terms in ΔG for High Spin-Low Spin Transition in FeO, as a Function of Applied Pressure (Energies in KK)

P (Kbar)	$-T\Delta S_m$	$P\Delta V_m (SP^*)$	$P\Delta V(CS^{**})$	ΔE	$\Delta G(SP)$	$\Delta G(CS)$
100	0.7	-2.2	-0.4	13.2	11.7	13.5
200	0.7	-4.3	-0.8	11.4	7.8	11.3
300	0.7	-6.5	-1.2	9.5	3.7	9.0
400	0.7	-8.6	-1.7	7.4	-0.5	6.4
500	0.7	-10.8	-2.1	5.0	-5.1	3.6
600	0.7	-13.0	-2.5	2.3	-10.0	0.5
700	0.7	-15.1	-2.9	-0.6	-15.0	-2.8

* *SP, using Shannon and Prewitt (1969) high spin-low spin IR(Fe^{2+}) difference.*
** *CS, using Clack and Smith (1974) calculated $^5T_{2g} - {}^1A_{1g}$ FeF_6^{4-} iron-fluorine distance decrease.*

will be only about 0.7 KK, and will favor the high-spin form.

The difference in internal energy for the high-spin ($^5T_{2g}$) and low-spin ($^1A_{1g}$) states of FeO_6^{10-} cannot be reliably evaluated from differences of SCF xα statistical total energies because the $2t_{2g}\uparrow - 3e_g\uparrow$ splitting is known to be exaggerated by the calculation. A reasonably accurate value for the internal energy difference can be obtained from the crystal field expressions of Griffith (1961) and from experimental data. The $^5T_{2g} - {}^1A_{1g}$ internal energy difference is $5B + 8C - 2\Delta$. Strens (1966) estimated $5B + 8C$ as 24.0 KK using $C = 3.7 B$ and

$$\frac{B \text{ oxide}}{B \text{ free-ion}} = \beta = 0.65.$$

Although accurate B and C values are still not available for Fe^{2+} oxides, the most recent compilation of spectroscopic data (Allen and Warren, 1971) gives $B_{\text{free ion}} = 917$ cm^{-1} and $C/B = 4.41$ for Fe^{2+} and $\beta \simeq 0.93$ for the Mn^{2+} oxides. Assuming a decrease to $\beta \simeq 0.90$ for the Fe^{2+} oxides, we recalculate $5B + 8C$ to be 33.3 KK.

Assuming $5B + 8C$ to change very slowly with $R(\text{Fe-O})$ and evaluating Δ as a function of R from the Wood and Strens crystal-field model and from the FeO compressibility data of Clendenen and Drickamer (1966), we find ΔE to be given by the equation:

$$\Delta E(\text{KK}) = 33.3 - 2(9.26)\left(\frac{2.152}{2.152 - .35P \text{ (mb)}}\right)^5$$

where 2.152 is the 1 atm Fe-O distance in FeO and $0.35P$(mb) is the distance decrease caused by pressure. Assuming $-T\Delta S_m$ to be constant at about 0.7 KK we obtain the values of ΔE, $-T\Delta S_m$, $P\Delta V_m$ and ΔG as a function of P given in Figure 4. Two different sets of values are given for $P\Delta V_m$ and ΔG, corresponding to the choice of Shannon and Prewitt or Clack and Smith values for the change in $R(\text{Fe-O})$ at the transition point. The Shannon and Prewitt value leads to a prediction of spin pairing between 300–400 kbar, while the Clack and Smith value predicts 600–700 kbar for the transition pressure. Pressures of 700 kbar are easily attainable in the earth's lower mantle. However at such depths the $-T\Delta S_m$ term would increase by about an order of magnitude, perhaps leading to positive ΔG values even at these high pressures. In the laboratory FeO apparently does not spin-pair below 300 kbar (Clendenen and Drickamer, 1966) since no discontinuity is observed in lattice parameters. However, in (future) experimental studies at higher pressures the small calculated decrease in $R(\text{Fe-O})$ must be kept in mind in evaluating the experimental results; the discontinuity in lattice parameter at the transition point may be so small as to be unobservable. Magnetic or Mössbauer data may therefore be required to identify the spin transition.

Effect of changes in R(Mg-O) upon the electronic structure of magnesium oxides

It is of some interest to look briefly at the effect of pressure on more ionic oxides. For the case of Mg in octahedral coordination with oxygen, the effect of distance variation upon electronic structure is substantially smaller than for the case for Fe. Decreasing

the Mg–O distance from 2.12 to 1.92 Å increases the valence region width (separation of the $1t_{1g}$ and $5t_{1u}$ orbitals) only from 2.5 to 3.3 eV. This increase is closely comparable to the calculated increase in width of the valence region between MgO_6^{10-}, $R = 2.12$ Å and AlO_6^{9-}, $R = 1.91$ Å. The electron distribution in the orbitals is also affected very little by this substantial change in Mg–O distance. These results indicate that relatively little change will occur in MgO bonding upon application of high pressure. Si–O bonds are quite rigid and are therefore compressed little at high pressure and the more compressible MgO_6 group shows little change in electronic structure at reduced R. Therefore, it is clear that any major changes in mineral electronic structure at high pressure must occur in the transition metal-oxygen polyhedra.

Conclusion

The SCF-Xα SW method yields the ordering of the minority spin crystal-field type orbitals in square planar FeO_4^{6-} as $d_{x^2-y^2} > d_{xy} > d_{xz,yz} > d_{z^2}$, in agreement with experiment. However, the calculated crystal field splittings are somewhat larger than the experimental values. The amont of $4s$, $4p$ covalency in the square planar ion is found to be much smaller than in tetrahedral or octahedral coordination, thus partially explaining the instability and consequent rarity of square planar Fe^{2+}. Substantial differences in Mössbauer isomer shift and optical spectra are predicted for the quintet and singlet states of FeO_4^{6-} at $R = 2.003$ Å. However, the predicted changes are not consistent with the changes in the optical spectra observed above 26 kbar. Direct simulation of the FeO_4^{6-} electronic structures at high pressure using SCF Xα calculations at $R = 1.98$ and 1.93 Å indicates that a quintet → singlet transition will not occur. Nevertheless, a failure to predict accurately the high pressure optical spectrum using the parameterized crystal field model demonstrates that the change in optical and Mössbauer properties above 26 kbar is still not quantitatively understood.

SCF-Xα calculations on Fe^{2+} and Fe^{3+} oxides at R(Fe–O) values of 2.17, 2.06, and 1.95 Å show: (1) increased crystal field splittings at small R, consistent with the R^{-5} law; (2) initial increases, followed by decreases for Fe^{2+} in spin-spin splittings; (3) initially increasing $O^{2-} \rightarrow M$ charge transfer energies, again followed by decreases for Fe^{2+} at smaller R; and (4) a rise in the crystal-field orbital baricenter and a lowering of bonding orbital energies at small R.

Appendix

The SCF Xα SW calculations employed α values of 0.7115, 0.7445 and 0.738 for Fe, O, and the interatomic and outer sphere regions, respectively. Sphere radii for $D_{4h}FeO_4^{6-}$ at $R = 2.03$ Å were 0.97, 1.06, 3.09, and 2.03 for the Fe, O, outer and Watson spheres, respectively, and were scaled down uniformly for the smaller Fe–O distances. FeO_6^{10-} and FeO_6^{9-} sphere radii were 1.04, 1.13, 3.30, and 2.17 Å, respectively, for $R = 2.17$, and were scaled down uniformly for the shorter Fe–O distances.

References

ABU-EID, R.M. (1974) Absorption spectra of transition metal-bearing minerals at high pressures. *Nato Adv. Study Institute, Petrophysics: The Physics and Chemistry of Minerals and Rocks.*

——H.K. MAO, AND R.G. BURNS ((1973) Polarized absorption spectra of gillespite at high pressure. *Carnegie Inst. Wash. Year Book,* 1972–73, 564–567.

AHRENS, T.J., AND Y. SYONO (1967) Calculated mineral reactions in the earth's mantle. *J. Geophys. Res.* **72,** 4181–4188.

ALLEN, G.C., D.W. CLACK, AND M.S. FARRIMOND (1971) Molecular orbital calculations on transition-metal complexes, Part III. Hexafluorometallate (III) and ⁻(IV) ions. *J. Chem. Soc. (A),* 2728–2733.

——, AND K. D. WARREN (1971) The electronic spectra of the hexafluoro complexes of the first transition series. *Structure and Bonding,* **9,** 49–138.

BALCHAN, A.S., AND H.G. DRICKAMER (1959) Effect of pressure on the spectra of olivine and garnet. *J. Appl. Phys.* **30,** 1446–1447.

BASCH, H., AND H.G. GRAY (1967) Molecular orbital theory for square-planar metal halide complexes. *Inorg. Chem.* **6,** 365–369.

BENTLEY, W.H., AND H.G. DRICKAMER (1961) Effect of pressure on the spectra of MnO_4^- and CrO_4^{-2}. *J. Chem. Phys.* **34,** 2200.

BURNS, R.G. (1970) *Mineralogical Applications of Crystal Field Theory.* Cambridge Univ. Press, Cambridge, England.

——, M.G. CLARK, AND A.J. STONE (1966) Vibronic polarization in the electronic spectra of gillespite, a mineral containing ion (II) in square planar coordination. *Inorg. Chem.* **5,** 1268–1272.

CLACK, D.W., AND W. SMITH (1974) Molecular orbital calculations on transition metal complexes. Part VIII. Potential energy curves for some $3d6$ complexes and their relation to Tanabe-Sugano diagrams. *J. Chem. Soc.,* p. 2015–2020.

CLENDENEN, R.L., AND H.G. DRICKAMER (1966) Lattice parameters of nine oxides and sulfides as a function of pressure. *J. Chem. Phys.* **44,** 4223–4228.

DRICKAMER, H. G., AND C. W. FRANK (1973) *Electronic Transitions and the High Pressure Chemistry and Physics of Solids.* Chapman and Hall, London.

ELLIS, D. E., AND F. W. AVERILL (1974) Electronic structure of FeCl₄ anions in .the Hartree-Fock-Slater approximation. *J. Chem. Phys.* **60,** 2856–2864.

FYFE, W.S. (1960) The possibility of *d*-electron coupling in olivine at high pressure. *Geochim. Cosmochim. Acta*, **19,** 141–143.

GAFFNEY, E.S. (1972) Crystal field effects mantle minerals. *Phys. Earth Planet. Interiors*, **6,** 385–390.

GRIFFITH, J.S. (1961) *The Theory of Transition Metal Ions.* Cambridge Univ. Press, Cambridge, England.

HUGGINS, F.E. (1974) The crystal chemistry of iron at high pressures: Mössbauer data. *Am. Geophys. Union Meet*, Spring 1974; *EOS,* **55,** 463.

HUSH, N.S. (1968) Homogeneous and heterogeneous optical and thermal charge transfer. *Electrochim. Acta,* **13,** 1005–1023.

JOHNSON, K.H. (1973) Scattered wave theory of the chemical bond. *Adv. Quant. Chem.* **7,** 143–185.

———, AND U. WAHLGREN (1972) Determination of the electronic structures of metal complexes by the SCF-Xα scattered-wave method. *Int. J. Quantum Chem., Symposium #6,* 243–256.

LEWIS, G.N., AND M. RANDALL (1961) *Thermodynamics,* revised by K.S. Pitzer and L. Brewer, McGraw-Hill, New York.

MAO, H.K., AND P.M. BELL (1972) Electrical conductivity and the red shift of absorption in olivine and spinel at high pressure. *Science,* **176,** 403–406.

———, AND ——— (1974) Crystal field effects of trivalent Ti in fassaite from the Pueblo de Allende meteorite. *Carnegie Inst. Wash. Year Book,* 488–492.

MESSMER, R.P., L.V. INTERRANTE, AND K.H. JOHNSON (1974) Electronic structure of square planar transition metal complexes. I. The PtCl₄⁻² and PdCl₄⁻² ions. *J. Am. Chem. Soc.* **96,** 3847–3854.

PABST, A. (1943) Crystal structure of gillespite, BaFeSi₄O₁₀. *Am. Mineral.* **28,** 372–390.

SHANKLAND, T.J., A.G. DIBA, AND A. WORONOW (1974) Pressure shifts of optical absorption bands in iron-bearing garnet, spinel, olivine, pyroxene, and periclase. *J. Geophys. Res.* **79,** 3273–3282.

SHANNON, R.D., AND C.T. PREWITT (1969) Effective ionic radii in oxides and fluorides. *Acta Crystallogr.,* **B25,** 925–946.

SLATER, J.C. (1972) Statistical exchange correlation in the self-consistent field. *Adv. Quantum Chem.* **66,** 1-92.

STRENS, R.G.J. (1966) Pressure-induced spin-pairing in gillespite, BaFe(II)Si₄O₁₀. *Chem. Commun.* **21,** 777–778.

STRENS, R.G.J. (1969), The nature and geophysical importance of spin pairing in minerals of iron (II), in*The Application of Modern Physics to the Earth and Planetary Interiors,* Wiley-Interscience, London.

TOSSELL, J.A., D.J. VAUGHAN, AND K.H. JOHNSON (1974) The electronic structure of rutile, wustite, and hematite from molecular orbital calculations. *Am. Mineral.* **59,** 319–334.

VAUGHAN, D.J., J.A. TOSSELL, AND K.H. JOHNSON (1974) The bonding of ferrous iron to sulfur and oxygen in tetrahedral coordination: a comparative study using SCF Xα scattered wave molecular orbital calculations. *Geochim. Cosmochim. Acta,* **38,** 993–1005.

WAINWRIGHT, J.E. (1969) Joint Annu. Meeting Geol. Assoc. Canada and Mineral Assoc. Canada, p. 57.

WANG, P.J., AND H.G. DRICKAMER (1973) Transformation from tetrahedral to planar symmetry in CS₂CuCl₄ and CS₂CuBr₄ at high pressure. *J. Chem. Phys.* **59,** 559–560.

WILLET, R.D., J.A. HAUGEN, J. LESBACK, AND J. MORREY (1974) Thermochromism in Cu(II) chlorides. Coordination geometry changes in CuCl₄⁻² anions. *Inorg. Chem.* **13,** 2510–2513.

WOOD, B.J., AND R.G.J. STRENS (1972) Calculation of crystal field splittings in distorted coordination polyhedra: spectra and thermodynamic properties of minerals. *Mineral. Mag.* **38,** 909–917.